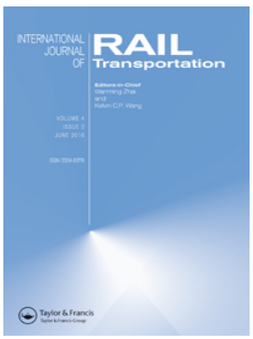

International Journal of Rail Transportation

ISSN: 2324-8378 (Print) 2324-8386 (Online) Journal homepage: http://www.tandfonline.com/loi/tjrt20

Effect of particle intrusion on rail seat load distributions on heavy haul freight railroads

Matthew J. Greve, Marcus S. Dersch, J. Riley Edwards, Christopher P.L. Barkan, Jose Mediavilla & Brent Wilson

To cite this article: Matthew J. Greve, Marcus S. Dersch, J. Riley Edwards, Christopher P.L. Barkan, Jose Mediavilla & Brent Wilson (2016) Effect of particle intrusion on rail seat load distributions on heavy haul freight railroads, International Journal of Rail Transportation, 4:2, 98-112, DOI: 10.1080/23248378.2016.1157048

To link to this article: http://dx.doi.org/10.1080/23248378.2016.1157048

INTERNATIONAL JOURNAL OF RAIL TRANSPORTATION, 2016
VOL. 4, NO. 2, 98–112
http://dx.doi.org/10.1080/23248378.2016.1157048

Taylor & Francis
Taylor & Francis Group

Effect of particle intrusion on rail seat load distributions on heavy haul freight railroads

Matthew J. Greve[a], Marcus S. Dersch[a], J. Riley Edwards[a], Christopher P.L. Barkan[a], Jose Mediavilla[b] and Brent Wilson[c]

[a]Rail Transportation Engineering Center, University of Illinois at Urbana-Champaign, Urbana, IL, USA; [b]RPS Inc., Kansas, MO, USA; [c]Amsted Rail, Granite City, IL, USA

ABSTRACT

The rail seat load distribution is critical for analysing failure mechanisms associated with rail seat deterioration (RSD), the degradation of concrete surface at the sleeper rail seat. RSD can lead to wide gauge, cant deficiency, and an increased risk of rail rollover. Previous experimentation with matrix-based tactile surface sensors (MBTSS) at the University of Illinois Urbana-Champaign (UIUC) has yielded concern regarding the feasibility of crushing of the concrete material at the rail seat. This paper examines data collected from laboratory experimentation in which the particle size, particle intrusion, vertical rail seat load, and lateral over vertical force ratio were varied to generate extreme loading environments. No pressures exceeded the concrete compressive strength. However, certain loading scenarios yielded pressures exceeding the concrete fatigue strength. It was therefore concluded that accumulated crushing damage due to a high number of repeated load applications is a feasible failure mechanism of RSD initiation.

ARTICLE HISTORY
Received 18 December 2015
Accepted 17 February 2016

KEYWORDS
Concrete sleeper; rail seat deterioration; rail seat abrasion; rail seat pressures; rail seat load distribution; particle intrusion; crosstie design

1. Introduction

As the demand in North America for high-performance, low-maintenance railroad infrastructure continues to grow, concrete sleepers and elastic fastening systems are becoming increasingly common. Concrete sleepers are typically used in areas of high curvature and steep grades on lines that experience high-speed or heavy axle load traffic [1]. Because of the increasingly common application of concrete sleepers and elastic fastening systems in these high-demand environments, it is important to understand the factors contributing to common performance failures of concrete sleepers and fastening systems. One of the most common failures of concrete sleepers is the degradation of the concrete material directly below the rail, in the area of the sleeper known as the rail seat. This degradation is commonly referred to as rail seat deterioration (RSD), or rail seat abrasion (RSA) [2]. Figure 1 illustrates a typical instance of RSD, with the depth of wear increasing towards the field side of the rail seat. RSD has become a problematic failure for concrete sleepers since it was first observed in the 1980's, and is often found in regions of steep grades, high curvature, and in the presence of moisture [1]. If left untreated, RSD

CONTACT Marcus S. Dersch mdersch2@illinois.edu

Figure 1. Typical rail seat deterioration (RSD) wear pattern.

may lead to accelerated wear of the fastening system, wide gauge, excessive rail cant, and an increased risk of derailment due to rail rollover [1].

According to a survey of North American railroad industry representatives, RSD is considered the most critical problem with concrete sleepers and fastening systems and was also ranked as the area most in need of additional research [3]. As part of a larger research project funded by the Federal Railroad Administration (FRA) investigating common failures with concrete sleepers and elastic fastening systems, researchers at the University of Illinois at Urbana-Champaign (UIUC) are investigating the failure modes associated with RSD. Previous research has identified five failure mechanisms that may result in RSD: abrasion, crushing, freeze-thaw cracking, hydro-abrasive erosion, and hydraulic pressure cracking [1]. Of these five failure mechanisms, four are affected by the distribution of loads on the sleeper rail seat, the exception being freeze-thaw cracking. Therefore, researchers at UIUC have undertaken an effort to better understand the distribution of the rail seat load, the factors that affect it, and its effect on RSD. Previous research has highlighted the effect of pad modulus, fastening system type, loading environment, RSD, and fastener wear on the rail seat load distribution [4–6]. Researchers at UIUC hope to incorporate the findings on RSD failure mechanisms with findings from other research to generate a framework for the mechanistic design of concrete sleepers and their fastening systems, in which components are designed from expected outputs and observed relationships. It is believed that such a design approach would establish a clearer procedure for designing sleepers and fastening systems, resulting in fewer service failures and higher reliability of the track structure and its components [5].

2. Crushing as an RSD failure mechanism

Crushing is defined as damage to the sleeper rail seat resulting from pressures exceeding the strength of the concrete material [1]. In North America, the minimum recommended design, 28-day compressive strength is 48 MPa (7,000 psi) [2]. Although the achieved 28-day compressive strength can exceed 76 MPa (11,000 psi), this study will consider the marginal case of a rail seat with a compressive strength of 48 MPa (7,000 psi) [1].

Experimentation conducted at the Volpe National Transportation Systems Center (Volpe) suggests that crushing may be a feasible failure mechanism for RSD. To investigate several passenger train derailments caused by RSD, Volpe utilized a NUCARS™ model to obtain the magnitudes of vertical and lateral load and location of the wheel/rail contact patch. This information was then applied to an empirical model, which treats the rail as a footing on an elastic foundation. The findings of this research suggest that pressures exceeding 110 MPa (16,000 psi) may be possible [7]. However, the analysis was performed under several 'worst-case' assumptions. The analysis neglected the rotational restraint provided by the elastic fasteners, and assumed that the rail pad provided no distribution of load from the rail. These assumptions may therefore not accurately represent typical field conditions, and may simulate only the most extreme cases of RSD and fastening system deterioration. Further, the highest pressures observed in previous research conducted at UIUC did not exceed 30 MPa (4,400 psi) [4–6]. This value is far below the minimum theoretical threshold for crushing, 48 MPa (7,000 psi), and experimentation was therefore undertaken with matrix-based tactile surface sensors (MBTSS) to generate extreme rail seat pressures via particle intrusion at the sleeper rail seat.

3. Instrumentation technology

To characterize the distribution of load at the sleeper rail seat, researchers at UIUC have utilized MBTSS. The MBTSS system used by UIUC is manufactured by Tekscan® Inc. and consists of rows and columns of conductive ink which, when pressed together by a load applied normal to the contact plane, output a change in resistivity at each intersection of a row and a column. This output, termed a 'raw sum', can be interpreted as the pressure exerted on the sensor at a given intersection when given the total applied load. MBTSS simultaneously outputs the area over which this load is applied. This is termed the 'contact area' of the load and is calculated from the number of sensing locations that indicate an applied load. Data are collected from the entire sensing area at a maximum rate of 100 Hz. The data are calibrated during analysis using a known or assumed input load.

Previous experimentation at the University of Kentucky (UK) and UIUC has shown that MBTSS are susceptible to shear and puncture damage. To protect the sensors, layers of biaxially-oriented polyethylene terephthalate (BoPET) and polytetrafluoroethylene (PTFE) are secured to both sides of a sensor that has been trimmed to fit the rail seat. The assembly is then calibrated on a loading frame between two steel platens according to manufacturer recommendations. After calibration, the assembly is installed between the rail pad assembly and the concrete sleeper rail seat (Figure 2) [8]. Figure 3 shows a photograph of the sensor assembly installed in a rail seat (a) and the sensor connected to a computer during experimentation (b).

4. Laboratory experimentation

Experimentation was conducted at UIUC's Research and Innovation Laboratory (RAIL) at Schnabel utilizing the Pulsating Load Testing Machine (PLTM), which is owned by RPS, Inc. The PLTM is a biaxial loading frame designed to perform

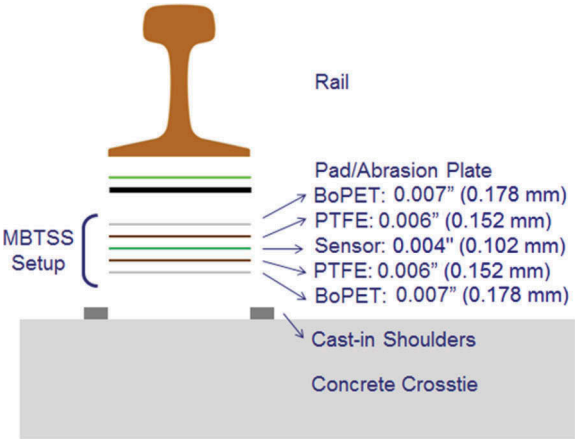

Figure 2. MBTSS layers and thicknesses.

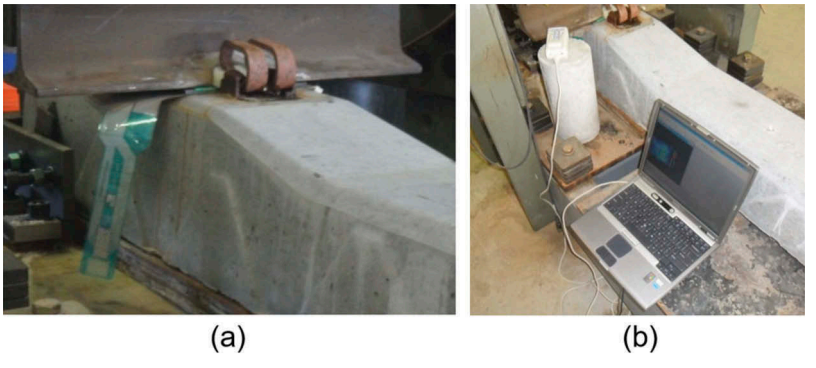

Figure 3. MBTSS assembly within system (a) and attached to computer (b) during experimentation.

AREMA Test 6, a Wear and Abrasion test, on a single rail seat with a complete fastening system assembly. The PLTM is equipped with one vertically-oriented 245 kN (55, 000 lb) actuator and one laterally-oriented 156 kN (35,000 lb) actuator. The actuators can be controlled independently by either force or displacement. For these experiments, force control was used. Figure 4 shows an example experiment installed on the PLTM.

In order to develop an experimental matrix which would generate extreme rail seat pressures, the size and amount of particles applied to each rail seat were varied. Locomotive sand meeting AAR specification M-916 – 51 was used to represent typical particle intrusion, as practical experience and the AREMA Test 6 procedure indicate that particles typically found at the rail pad-rail seat interface are of comparable size. To generate more extreme pressures, virgin Class B crushed stone ('B-Stone') aggregate from the UIUC concrete laboratory was used to simulate debris from deterioration of the concrete at the rail seat. Figure 5 shows the grain size distribution of the aggregate after all material retained at or above the #4 sieve was removed (14% of the total sample by weight).

Figure 4. Example experimental set-up using Pulsating Load Testing Machine (PLTM).

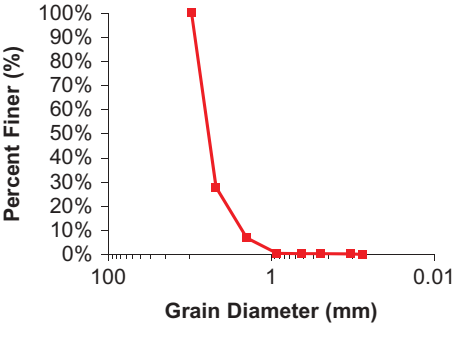

Figure 5. Concrete aggregate grain size distribution.

Previous experimentation has shown that the portion of the rail seat not more than 2.54 cm (1 in) from the field-side shoulder is the region of the rail seat which is most sensitive to changes in the rail seat load distribution [5]. Therefore, it was decided to also vary the portion of the rail seat over which the particles were applied. Figure 6 shows the particle distributions that were considered. To evaluate the effect of the loading environment and provide a control against which the particle trials could be compared, the rail seats were first tested with no particle intrusion (Figure 6a). To

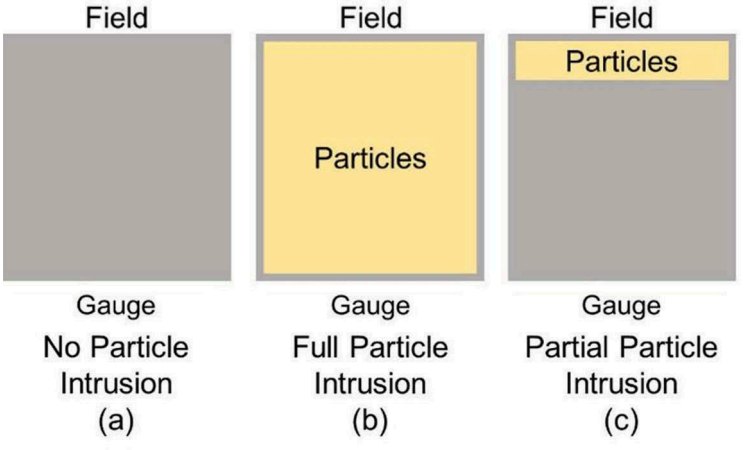

Figure 6. Illustration of particle distribution cases.

represent typical particle intrusion, 15 mL (3.0 teaspoons) of material were distributed evenly over the entire rail seat (Figure 6b). To simulate a more extreme case, 2.5 mL (0.5 teaspoons) of material were distributed evenly over the 2.54 cm (1 in) of the rail seat closest to the field side, as described above (Figure 6c). It was hypothesized that this uneven distribution of particles would create an effective difference in height across the rail seat, resulting in a greater proportion of the rail seat load imparted on the area of the rail seat already known to be most sensitive to changes in rail seat load.

This combination of particle size and region of intrusion leads to five experimental cases: No Fines (the control case), Partial Sand (sand applied to the field side of the rail seat), Full Sand (sand applied to the entire rail seat), Partial Aggregate (B-Stone aggregate applied to the field side of the rail seat), and Full Aggregate (B-Stone aggregate applied to the entire rail seat).

In field conditions, it is rare that a single rail seat will carry the entire vertical load applied by a single wheel. Instead, the vertical wheel load is often distributed across five or more sleepers, with the rail seat directly below the point of loading carrying the largest proportion of the load [9]. An extensive literature review and previous field experimentation have shown that average values for the rail seat load directly below point of loading are typically close to 50% of the total vertical wheel load. However, this value may vary significantly, predominately due to the support conditions under the rail seat in relation to that of neighbouring rail seats [2]. The magnitude of vertical load applied in this experimentation was therefore varied to capture this behaviour, with testing conducted at 44.5 kN (10,000 lb), 88.9 kN (20,000 lb), and 133 kN (30,000 lb). These values were chosen to represent 25%, 50%, and 75% of 178 kN (40,000 lb), which represents a 95th percentile nominal vertical wheel load in North American heavy haul freight service [10]. At each magnitude of vertical load, the Lateral/Vertical (L/V) Force Ratio was also varied from 0.0 to 0.6, to simulate varying degrees of curvature. Five seconds of data were captured under static loading for each combination of vertical and lateral load, and were averaged during analysis to reduce transient noise in the data. Due to the design of the PLTM, longitudinal forces simulating the effect of traction and

braking on steep grades could not be replicated in this experimentation. Therefore, additional tests are required to evaluate the effect of tractive forces on the distribution of load at the rail seat.

The RPS P2000 fastening system was used in this experimentation. All clips were applied new, and discarded when removed to eliminate variability due to reduced toe load from fastener wear. The same two-part pad assembly and insulators were used for all experimentation to eliminate thickness variations within manufacturing tolerances. The pad assembly and insulators were lightly used in previous experimentation but were undamaged prior to installation. Before each application of particles, the rail seat was cleaned with a handheld broom to prevent contamination from the prior particle intrusion case (e.g. removing sand prior to experimentation with aggregate). Three separate trials were conducted for each combination of particle size, intrusion region, vertical load, and lateral load. The results presented in this paper represent an average of the three corresponding data points, except as noted. Replicates were collected to assess the variability induced by particle intrusion, but the rail seat load distribution was found to behave consistently for repeated trials with identical experimental conditions.

5. Results

During experimentation, researchers noted that the presence of aggregate at the rail seat significantly increased the difficulty of assembling the fastening system. Due to the effective increase in height of the rail base above the rail seat, the insulators developed a tendency to become unseated during clip application. Additional rotational restraint of the rail was required to enable the application of both fasteners. Upon disassembly of the fastening system following experimentation with the crushed stone aggregate, the particles were found to have been pulverized during experimentation, resulting in reduced particle size as shown in Figure 7. Despite the pulverization of the aggregate, the qualitative behaviour of the rail seat load distribution did not appear to change as a result of the effective decrease in particle size. Due to the small sample size, a sieve analysis was not run on the pulverized material.

In order to prevent failure of the fastening system, experimentation was halted when the rail seat load became concentrated solely on the half of the rail seat closest to the field-side shoulder (i.e. if the gauge side of the rail seat was completely unloaded). Experience has shown high lateral loads tend to result in this concentration, which precedes the plastic yield failure of the gauge-side clip. This threshold was reached at approximately 0.56 L/V force ratio under a 133 kN (30,000 lb) vertical load during experimentation both with no fines present and in the Full Sand case. When aggregate was placed on the field side of the rail seat, the target 0.6 L/V force ratio was achieved at all three tested vertical load magnitudes. It is hypothesized that the improved tolerance of high lateral loads was due to an effective increase in rail cant caused by the aggregate elevating the field side of the rail base. When aggregate was placed on the entire rail seat, experimentation was halted at 0.58 L/V under an 88.9 kN (20,000 lb) vertical load and 0.5 L/V under a 133 kN (30,000 lb) vertical load due to the previously described unloading of the gauge side. It is hypothesized that the effective increase in height of the rail base, which led to the aforementioned difficulty with assembling the fastening

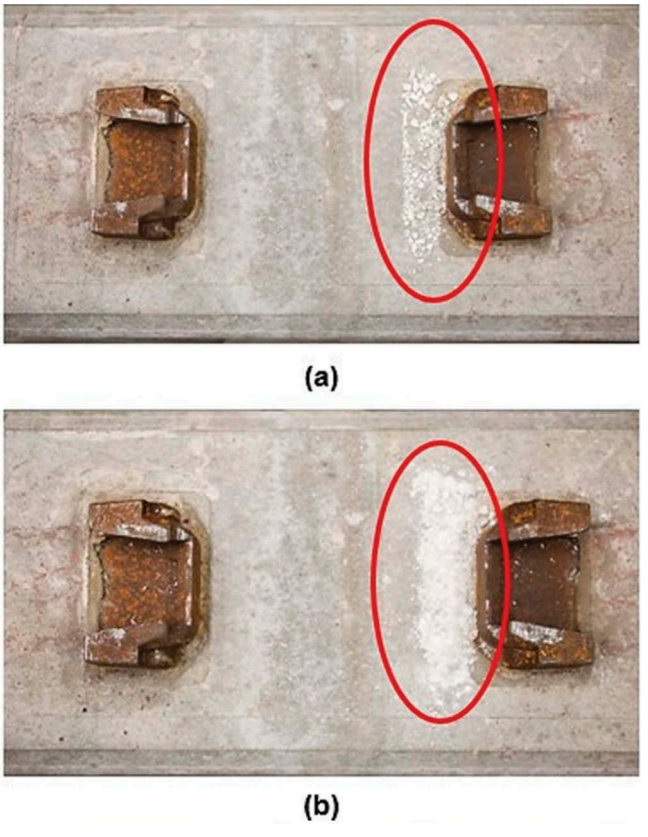

Figure 7. Aggregate (circled) before (a) and after (b) Partial Aggregate experiments.

system, may have changed the magnitude and direction of the resultant force applied by the fastener toe load, leading to a decrease in rail rotational restraint.

5.1 *Qualitative analysis*

Figure 8 compares the qualitative effect of both L/V force ratio and particle intrusion on rail seat load distributions. The first series represents a rail seat load uniformly distributed across the entirety of a clean sleeper rail seat. By definition, this assumption does not account for changes in L/V force ratio. The remaining five series illustrate each of the experimental cases for particle intrusion: clean rail seat (no particle intrusion), sand intrusion on the field side of the rail set, sand intrusion on the entire rail seat, aggregate intrusion on the field side of the rail seat, and aggregate intrusion on the entire rail seat.

A non-uniform distribution of load was observed in all five experimental cases, with the variation in particle size and extent of intrusion affecting the magnitude of non-uniformity. The primary effect of particle size was on regularity of the load distribution. Larger aggregate particles produced greater variation in measured load at adjacent sensing locations, as represented by the 'peaks' of warmer colours evident in the Full Aggregate case. The primary effect of the extent of particle intrusion was on the portion

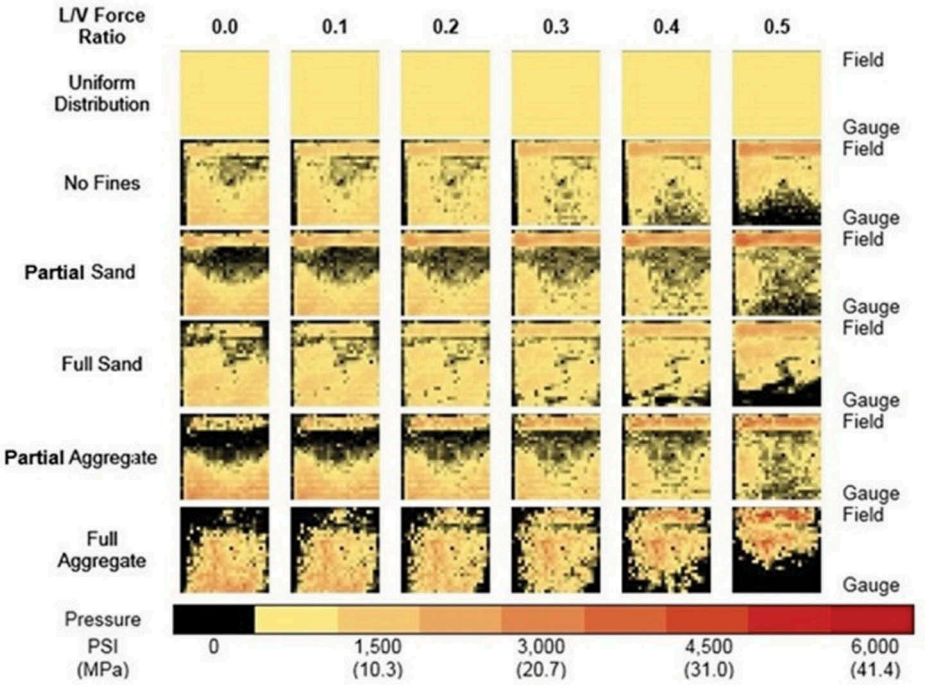

Figure 8. Qualitative comparison of rail seat load distributions under 133 kN (30,000 lb) vertical wheel load at varying L/V force ratio.

of load applied to the region of the rail seat not more than 2.54 cm (1 in) from the field-side shoulder. The intrusion of particles exclusively in this region leads to a gap in the load distribution at lower L/Vs that is not present under the intrusion of particles across the entire rail seat. Moreover, experimentation with sand particles suggests that in the Partial Sand case, a greater portion of the rail seat load was applied to the field side of the rail seat than in the Full Sand case.

5.2 *Quantitative analysis*

Figure 9 summarizes the effect of particle intrusion on contact area (the area over which the rail seat load is distributed) when subjected to increasing L/V force ratio under a constant 133 kN (30,000 lb) vertical load. This vertical load was selected to focus the analysis as it consistently yielded the most extreme pressures. In the No Fines, Partial Sand, and Full Sand cases, more than 90% of the rail seat is engaged at low L/V force ratios. The contact area remains relatively constant until a 0.4 L/V force ratio is reached, with the presence of sand introducing slightly higher contact areas than the No Fines case. Beyond 0.4 L/V, the three cases experienced a rapid loss of contact area. When experimentation was halted at approximately 0.56 L/V, the No Fines, Partial Sand, and Full Sand cases exhibited a 38%, 37%, and 41% reduction in contact area, respectively, relative to the baseline contact area observed at 0.0 L/V in the No Fines case. This suggests that the intrusion of locomotive sand did not significantly affect the

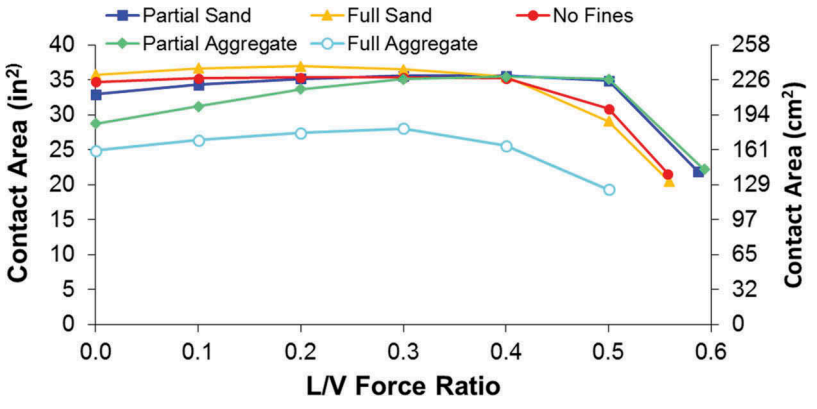

Figure 9. Loss of contact area under 133 kN (30,000 lb) vertical load.

ability of the fastening system to reduce rail seat load concentration through rotational restraint.

As shown qualitatively in Figure 8, the presence of aggregate at the concrete sleeper rail seat generates an overall reduction in contact area. Both aggregate cases exhibited a lower initial contact area at 0.0 L/V. When compared to the baseline contact area, observed at a 0.0 L/V force ratio in the No Fines case, 17% less area was loaded in the Partial Aggregate case, and 28% less was loaded in the Full Aggregate case. Both aggregate cases then showed a gradual increase in contact area before reaching a critical L/V force ratio. Beyond this threshold, both experimental cases exhibited rapid reductions in contact area. In the Partial Aggregate case, contact areas comparable to those observed in the No Fines case were achieved at L/V force ratios between 0.3 and 0.5 L/V. As previously mentioned, the Partial Aggregate case was the only experimental case to achieve the target L/V force ratio of 0.6 under a 133 kN (30,000 lb) vertical load, at which point the contact area was measured to be 36% less than that at the baseline of 0.0 L/V in the No Fines case. The Full Aggregate case, by comparison, achieved a maximum contact area 19% lower than the baseline contact area. When experimentation was halted at 0.5 L/V, the Full Aggregate case exhibited 44% less contact area than the baseline measurement at 0.0 L/V force ratio in the No Fines case. This suggests that, unlike in experiments utilizing locomotive sand, the introduction of aggregate particles affected the ability of the fastening system to resist rail rotation.

Figures 10 and 11 quantify the change in pressure as a result of the experimentation. There are three primary metrics by which rail seat pressures are typically analyzed: theoretical uniform pressure, average pressure, and maximum pressure. The theoretical uniform pressure is obtained by dividing the total rail seat load by the total rail seat area, and represents a rail seat load uniformly distributed across the entirety of the sleeper rail seat. The theoretical uniform pressure is included in both Figures 10 and 11 and serves as a theoretical minimum average pressure at a given vertical rail seat load. The average pressure is obtained by dividing the total rail seat load by the measured contact area, rather than the total rail seat area as used to calculate the theoretical uniform pressure. The maximum pressure is the highest pressure recorded by the MBTSS at a given combination of vertical load and L/V force ratio.

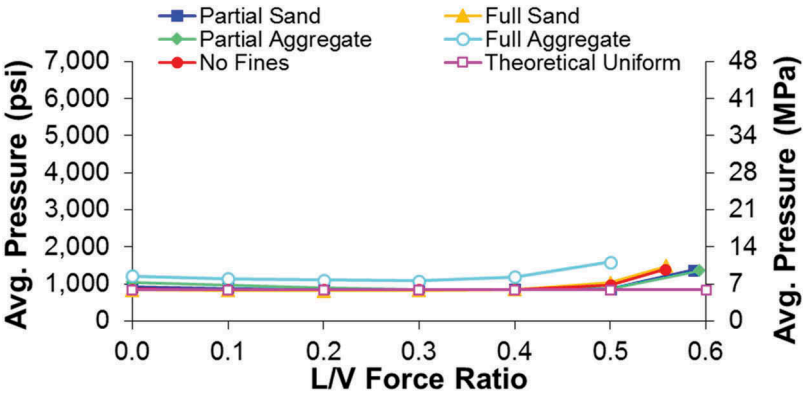

Figure 10. Increase in average pressure under 133 kN (30,000 lb) vertical load.

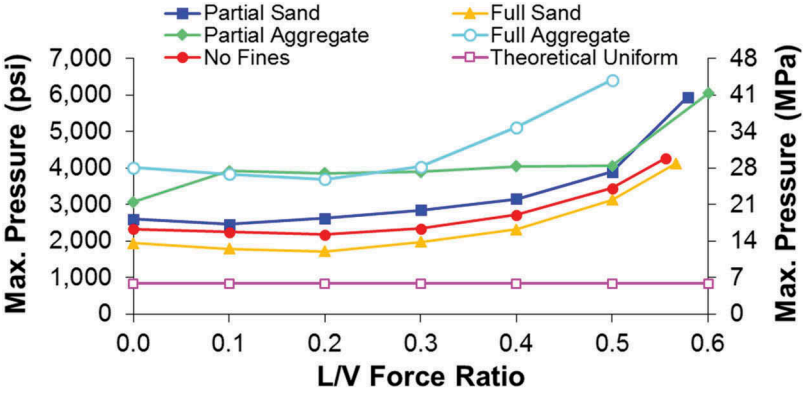

Figure 11. Increase in maximum pressure under 133 kN (30,000 lb) vertical load.

Figure 10 illustrates the effect of particle intrusion and L/V force ratio on the average rail seat pressure. Because average pressure is derived from contact area, the data series exhibit inverse behaviour when compared to the contact area data illustrated in Figure 9 (i.e. lower contact areas correlate to higher average pressures). Because the No Fines, Partial Sand, and Full Sand cases result in almost the entire rail seat being engaged in load transfer at low L/V force ratios, the average pressures plot very close to the theoretical uniform pressure. Below the aforementioned threshold of 0.4 L/V, the three cases yielded average pressures within 6% of the baseline average pressure observed at an L/V force ratio of 0.0 in the No Fines case. As contact area decreased above this threshold, the No Fines, Partial Sand, and Full Sand cases experienced an increase in average pressure of 61%, 51%, and 75%, respectively, resulting in average pressures 61%, 59%, and 71% higher, respectively, than the baseline average pressure.

Due to the reduced contact area measured in the presence of aggregate at the sleeper rail seat, the Partial Aggregate and Full Aggregate cases exhibited slightly higher average pressures than those observed on a clean rail seat or in the presence of sand. As contact area increased between 0.0 and 0.3 L/V force ratio in the Partial Aggregate case, the average pressure was reduced from 21% higher than the baseline average pressure to 1%

lower. Following the loss of contact area from 0.5 to 0.6 L/V, the average pressure increased 59%, resulting in an average pressure 58% higher than that recorded on a clean rail seat at 0.0 L/V force ratio. In the Full Aggregate case, the average pressure at 0.0 L/V was 40% higher than that measured in the baseline case, before experiencing a reduction as increasing L/V force ratio resulted in a greater portion of the rail seat engaged in load transfer. At 0.3 L/V, the average pressure observed in the Full Aggregate case was just 24% higher than the baseline average pressure, before again increasing as contact area was lost. At 0.5 L/V, when experimentation was halted, the Full Aggregate case had experienced an overall increase in pressure of 31%, resulting in values 84% higher than the average pressure on a clean rail seat at 0.0 L/V. The highest average pressure recorded was 11 MPa (1,587 psi), well below the theoretical minimum value at which crushing is theorized to occur (48 MPa).

Figure 11 illustrates the effect of particle intrusion and L/V force ratio on the maximum rail seat pressure. While the presence of sand resulted in contact areas slightly higher than those observed in the No Fines case, Figure 8 shows significant areas of the rail seat engaged in load transfer at lower pressures in the Partial Sand case. This, therefore, leads to higher maximum pressures than those seen in the No Fines and Full Sand cases. In both the Full Sand and No Fines cases, maximum pressures 58% higher than the baseline maximum pressure were observed at 0.56 L/V. In the Partial Sand case, maximum pressures recorded at 0.58 L/V were 154% higher than the baseline maximum pressure. The Partial Aggregate case resulted in behaviour similar to the Partial Sand case, with maximum pressures at 0.0 and 0.6 L/V force ratio ranging from 32% to 159% higher than the baseline maximum pressure, respectively. The Full Aggregate case consistently exhibited the highest maximum pressures at any given L/V force ratio, ranging from 72% to 175% higher than the baseline maximum pressure.

The highest maximum pressure recorded during experimentation was observed in the Full Aggregate case, with a maximum pressure of approximately 44 MPa (6,400 psi) achieved at 0.5 L/V force ratio. It is hypothesized that crushing of the B-Stone aggregate occurred at these high L/V force ratios, leading to reduced particle size which, in turn, led to similar results to the Partial Sand case at high L/V force ratios. Had the aggregate particles not failed, it is feasible that higher maximum pressures could have been observed. Further experimentation with stronger aggregate is needed to evaluate this hypothesis. The sensing resolution of the MBTSS also presents a limitation. Each sensing location is a square with sides 0.56 cm (0.22 in) in length. It is possible that there may have been regions smaller than the size of a single sensing location, where the applied pressures were higher than those observed in this study. Due to the limitations of the instrumentation, however, the data reflect the average pressure applied to each 0.31 cm^2 (0.0484 in^2) sensing location. Nonetheless, because the observed maximum pressures fall short of the design compressive strength of concrete used in the manufacture of concrete sleepers in North America (48 MPa), crushing damage due to a single load application is not expected in the presence of particle intrusion on a concrete rail seat with a new fastening system.

While this experimentation did not generate pressures exceeding the design compressive strength of the concrete, crushing damage as a result of repeated load applications may be feasible. The fatigue compressive strength of concrete is generally regarded as ranging from 50% to 60% of the ultimate compressive strength for high-load cycle

applications [11, 12]. A conservative estimate of the design fatigue compressive strength of concrete would, therefore, be 24 MPa (3,500 psi), or half of the design compressive strength. Figure 11 shows that at high L/V force ratios (above 0.4), the maximum pressures observed in the Partial Sand, Partial Aggregate, and Full Aggregate cases exceeded this threshold. This indicates that crushing damage to the concrete rail seat as a result of repeated load applications may indeed be feasible in cases of extreme particle intrusion and high rail seat loads.

Practical experience has shown that the actual compressive strength achieved in the manufacture of North American concrete sleepers can exceed 76 MPa (11,000 psi), nearly twice the highest pressure observed in this experimentation. Further, the reported concrete compressive strength is obtained from compressive tests on unreinforced concrete cylinders [2]. The confinement provided by the mass of concrete comprising the rail seat and the prestress provided by the sleeper reinforcement will further increase the actual compressive strength of the concrete at the sleeper rail seat, further increasing the pressure necessary to generate crushing. Although these factors further indicate that crushing due to a single load application may not be feasible, the data shown in Figure 11 suggest that crushing due to repeated load application may still be feasible in the most extreme cases (e.g. particle intrusion only on the field side of the rail seat). Further, previous laboratory experimentation has shown that fastener wear can lead to an increase in rail seat pressures [5]. In such cases, the accumulation of crushing damage to the concrete rail seat may be accelerated by the increase in maximum pressures.

6. Conclusions

In this experimentation, particle size, extent of intrusion, vertical rail seat load, and L/V force ratio were varied to generate realistically demanding loading environments. The distribution of loads at the sleeper rail seat was collected using MBTSS, and the data were analyzed to determine the effect of particle intrusion. While the presence of sand had little effect on the measured contact area, the presence of aggregate led to an average reduction of 23% at 0.0 L/V force ratio. An average 35% reduction in contact area due to high L/V force ratios was observed in all experimental cases. No average pressures were observed to be greater than 200% of the theoretical average pressure given a uniform distribution of rail seat load. While maximum pressures of 44 MPa (6,400 psi) were recorded in the most extreme loading cases, the minimum threshold to generate crushing, a proposed failure mechanism for RSD, as a result of a single load application, was not exceeded. Further, as mentioned previously, concrete sleeper manufacturers routinely achieve 28-day compressive strengths which exceed 76 MPa (11,000 psi), raising the practical threshold at which crushing is expected. Given that the achieved compressive strength of the concrete can exceed the design compressive strength by as much as 58%, crushing is, therefore, not expected to occur under the circumstances given. In extreme loading cases, however, the estimated design fatigue strength of the concrete, 24 MPa (3,500 psi) was exceeded. These findings indicate that crushing damage may be generated as a result of a large number of repeated load applications. It was, therefore, concluded that although crushing damage of concrete sleeper rail seats due to a single load application is not expected, crushing damage due to repeated load applications may be feasible in the presence of particle intrusion.

Acknowledgements

The published material in this report represents the position of the authors and not necessarily that of US DOT. Generous support and guidance has also been provided from the industry partners of this research: Union Pacific Railroad; BNSF Railway; National Railway Passenger Corporation (Amtrak); Amsted RPS/Amsted Rail, Inc.; GIC Ingeniería y Construcción; Hanson Professional Services, Inc.; and CXT Concrete Ties, Inc., and LB Foster Company. For providing direction, advice, and resources, the authors would like to thank Christopher Rapp from Hanson Professional Services, Inc, Mauricio Gutierrez from GIC Ingeniería y Construcción, Professor Jerry Rose and Graduate Research Assistant Jason Stith from the University of Kentucky, and Vince Carrara from Tekscan®, Inc. The authors would also like to thank Tim Prunkard and the Civil and Environmental Engineering (CEE) Machine Shop from the University of Illinois at Urbana-Champaign for their assistance in laboratory experimentation, and undergraduate research assistant Zachary Jenkins for his assistance in analyzing the data presented in this paper.

Disclosure statement

No potential conflict of interest was reported by the authors.

Funding

This research was primarily funded by Amsted RPS, who also supported the first two authors by a research grant. Additional support was provided by the National University Rail (NURail) Center, a US DOT-OST Tier 1 University Transportation Center. J. Riley Edwards has been supported in part by grants to the UIUC Rail Transportation and Engineering Center (RailTEC) from CN, CSX, Hanson Professional Services, and the George Krambles Transportation Scholarship Fund.

References

[1] Zeman JC. Hydraulic mechanisms of concrete-tie rail seat deterioration [M.S. Thesis]. Urbana (IL): University of Illinois at Urbana-Champaign; 2010.
[2] American Railway Engineering and Maintenance-of-Way Association. Manual for railway engineering. Lanham (MD): AREMA; 2014.
[3] Van Dyk BJ Characterization of loading environment for shared-use railway superstructure in North America (M.S. Thesis). Urbana (IL): University of Illinois at Urbana-Champaign; 2014.
[4] Rapp CT, Dersch MS, Edwards JR, et al. Measuring rail seat pressure distribution in concrete crossties: Experiments with matrix-based tactile surface sensors. Transport Res Rec. 2014;2374:190—200. doi:10.3141/2374-22.
[5] Greve MJ Quantification of rail seat load distribution on concrete crossties [M.S. Thesis]. Urbana (IL): University of Illinois at Urbana-Champaign; 2015.
[6] Greve MJ, Dersch MS, Edwards JR, et al. Examination of the effect of concrete crosstie rail seat deterioration on rail seat load distribution. Transport Res Rec. 2015;2476:1—7. doi:10.3141/2476-01.
[7] Choros J, Coltman MN, Marquis B. Prevention of derailments due to concrete tie rail seat deterioration. In: Proceedings of the ASME Joint Rail Conference & Internal Combustion Engine Spring Technical Conference. Pueblo (CO); 2007.
[8] Rapp CR, Edwards JR, Dersch MS, et al. Measuring concrete crosstie rail seat pressure distribution with matrix based tactile surface sensors. In: Proceedings of the ASME Joint Rail Conference. Philadelphia (PA); 2012.

[9] Hay WW. Railroad Engineering. 2nd ed. New York (NY): Wiley; 1982.
[10] Van Dyk BJ, Dersch MS, Edwards JR, et al. Load characterization techniques and overview of loading environment in North America. Transport Res Rec. 2014;2448:80–86. doi:10.3141/2448-10.
[11] El Shahawi M, Batchelor B. Fatigue of partially prestressed concrete. J Structural Eng. 1986;112(3):524—537. doi:10.1061/(ASCE)0733-9445.
[12] ACI Committee 215. Considerations for design of concrete structures subjected to fatigue loading. Detriot (MI): American Concrete Institute; 1992.